J. Membrane Biol. 125, 273–285 (1992)

The Journal of
Membrane Biology

Na^+ Transport and Impedance Properties of Cultured Renal (A6 and 2F3) Epithelia

N.K. Wills, R.K. Purcell, and C. Clausen†

Department of Physiology and Biophysics, University of Texas Medical Branch, Galveston, Texas 77550-2781, and †Department of Physiology and Biophysics, Center for Health Sciences, State University of New York at Stony Brook, Stony Brook, New York 11794-8861

Summary. Previous impedance analysis studies of intact epithelia have been complicated by the presence of connective tissue or smooth muscle. We now report the first application of this method to cultured epithelial monolayers. Impedance analysis was used as a nondestructive method for deducing quantitative morphometric parameters for epithelia grown from the renal cell line A6, and its subclonal cell line 2F3.

The subclonal 2F3 cell line was chosen for comparison to A6 because of its inherently higher Na^+ transport rate. In agreement with previous results, 2F3 epithelia showed significantly higher amiloride-sensitive short-circuit currents (I_{sc}) than A6 epithelia (44 ± 2 and $27 \pm 2\ \mu A/cm^2$, respectively). However, transepithelial conductances (G_T) were similar for the two epithelia (0.62 ± 0.04 mS/cm^2 for 2F3 and 0.57 ± 0.04 mS/cm^2 for A6) because of reciprocal differences in cellular (G_c) and paracellular (G_j) conductances. Significantly lower G_j and higher G_c values were observed for 2F3 epithelia than A6 ($G_j = 0.23 \pm 0.02$ and 0.33 ± 0.04 mS/cm^2 and $G_c = 0.39 \pm 0.16$ and 0.26 ± 0.10 mS/cm^2, respectively). Nonetheless, the cellular driving force for Na^+ transport (E_c) and the amount of transcellular Na^+ current under open-circuit conditions (I_c) were similar for the two epithelia.

Three different morphologically-based equivalent circuit models were derived to assess epithelial impedance properties: a distributed model which takes into account the resistance of the lateral intercellular space and two models (the "dual-layer" and "access resistance" models), which corrected for impedance of small fluid-filled projections of the basal membrane into the underlying filter support. Although the data could be fitted by the distributed model, the estimated value for the ratio of apical to basolateral membrane resistances was unreasonably large. In contrast, the other models provided statistically superior fits and reasonable estimates of the membrane resistance ratio. The dual-layer model and access resistance models also provided similar estimates of apical and basolateral membrane conductances and capacitances. In addition, both models provided new information concerning the conductance and area of the basolateral protrusions. Estimates of the apical membrane conductance were significantly higher for 2F3 (0.79 ± 0.23 mS/cm^2) than A6 epithelia (0.37 ± 0.07 mS/cm^2), but no significant difference could be detected for apical membrane capacitances (1.4 ± 0.04 and $1.2 \pm 0.1\ \mu F/cm^2$ for 2F3 and A6, respectively) or basolateral membrane conductances (3.48 ± 1.67 and 2.95 ± 0.40 mS/cm^2). The similar basolateral membrane properties for the two epithelia may be explained by their comparable transcellular Na^+ currents under open-circuit conditions.

We conclude that impedance analysis can be a highly useful and noninvasive method for deducing the membrane properties of cultured epithelial monolayers. The difference between A6 and 2F3 epithelia with respect to apical membrane Na^+ conductance and paracellular conductance may provide a useful tool for assessing the regulation of Na^+ transport and tight junctional proteins.

Key Words A6 · eithelium · impedance · amiloride · nystatin · cultured renal epithelia

Introduction

Impedance analysis has been successfully used as a noninvasive method for studying the membrane properties of epithelia (Clausen, Lewis & Diamond, 1979; Kottra & Fromter, 1984). A key advantage to this technique is that it provides a means for deducing quantitative morphological features of the epithelium such as the dimensions of the lateral intercellular space, or in the case of intestinal epithelia, the diameter of the crypt lumen (*cf.* Wills & Clausen, 1987). Since capacitance is proportional to membrane area (Cole, 1972), this technique has been particularly useful for measuring changes in membrane areas during ion transport regulation (Clausen, Machen & Diamond, 1983). Nonetheless, the presence of connective tissue or smooth muscle in intact epithelia can complicate the interpretation of impedance results.

In the present study, we applied impedance methods to cultured monolayers of renal epithelia. Cultured monolayers are technically advantageous for such studies since they consist of a single homogeneous cell layer and have a relatively simple morphology. Thus, series impedances arising from connective tissue, smooth muscle, or epithelial folding are eliminated. By combining this approach with DC equivalent circuit analysis techniques, we have

assessed the membrane properties of cultured renal epithelia from the A6 cell line and its subclonal cell line, 2F3.

The A6 cell line has recently become a popular model for studies of Na^+ transport regulation. Under short-circuit conditions, the transepithelial current (I_{sc}) is equivalent to the rate of net Na^+ absorption (Perkins & Handler, 1981; Fidelman & Watlington, 1987) and is mediated by amiloride-sensitive Na^+ channels in the apical membrane (Hamilton & Eaton, 1985; Olans, Sariban-Sohraby & Benos, 1984; Wills, Millinoff & Crowe, 1991). Na^+ transport in this epithelium is stimulated by several factors including vasopressin (Lang et al., 1986), aldosterone (Handler et al., 1981), and reduced serosal solution osmolarity (Wills et al., 1991). As originally reported by Verrey et al. (1987), aldosterone produces a larger stimulation of I_{sc} in 2F3 epithelia than A6 epithelia. Wills and Millinoff (1990) observed larger I_{sc} values for 2F3 than A6 epithelia both before and during aldosterone stimulation (basal I_{sc} values in unstimulated 2F3 epithelia averaged 44 $\mu A/cm^2$ compared to 23 $\mu A/cm^2$ for A6).

In the present study we sought to determine the membrane basis for this difference in the basal Na^+ transport rate. We asked the following questions: (i) Are the apical membrane surface areas or the density of conducting Na^+ channels in this membrane different for A6 and 2F3 epithelia? Specifically, are the capacitances or specific conductances (i.e., membrane conductance normalized to membrane area) significantly different? (ii) Do basolateral membrane properties or paracellular conductances differ for the two epithelia? If so, do these differences affect transepithelial Na^+ transport?

Materials and Methods

Cell Culture

A6 renal epithelial cells derived from *Xenopus laevis* were obtained from American Type Tissue Culture Collection (Rockville, MD) at passage 69. Cells from passages 74–79 were grown as confluent monolayers on permeable support systems (Millicell-HA: 0.45 μm pore size, 4.2 cm^2 area, Millipore, Bedford, MA) according to previously described methods (Wills and Millinoff, 1990). Cells were seeded at a density of 2.4×10^5 cells/cm^2 and fed three times weekly with a growth medium consisting of Dulbecco's Modified Eagle medium (amphibian formula: Gibco Laboratories, Grand Island, NY, catalogue no. 84-5022) supplemented with 40 mU/ml penicillin, 40 μg/liter streptomycin and 10% fetal calf serum (Hyclone Laboratories, Logan, UT; final solution osmolarity, 200 mOsm). Cells were maintained at 28°C in a humidified incubator gassed with 1% CO_2 in air, and experiments were performed after 10–18 days of incubation.

Experimental Chambers

To mount the epithelium in the experimental chamber, the epithelium and underlying filter paper were cut away from the culture plate insert using a razor blade or scalpel. The resulting disk was then placed on a ring of pins coated with vacuum grease (to minimize edge damage) and mounted between the chamber halves of a modified Ussing chamber (aperture area = 2 cm^2). The filter paper side was supported against a nylon mesh by a small hydrostatic gradient resulting from a slight excess of mucosal solution. Water jackets maintained the solutions in the chambers at a temperature of 28°C, and magnetic spin bars in the bottom of each chamber continuously stirred the solutions. In addition, tissues were continuously bubbled with 1% CO_2 in air to maintain the solution pH at 7.4.

Solutions

Sodium chloride Ringer's solution was designed to match the electrolyte composition of the culture medium and contained (in mM): 74.4 NaCl, 5.4 KCl, 8 $NaHCO_3$, 1.4 $CaCl_2$, 1.7 $MgSO_4$, 0.9 NaH_2PO_4, 5.5 glucose, 1 Na pyruvate, and 1 N-2-hydroxyethylpiperazine-N'-2-ethanesulfonic acid (HEPES). The solution pH was maintained at 7.4 and the osmolarity was 170 mOsm. Amiloride (a gift from Merck, Sharp, and Dohme) was prepared as a 10 mM stock solution in distilled water. Nystatin (Sigma, St. Louis, MO) was prepared as a 5 mg/ml stock solution (3,010 units/ml) in methanol or as a 50 mg/ml stock in DMSO. Microliter quantities of the stock solutions were added to the bathing solutions to achieve desired concentrations. For aldosterone-treated tissues, a stock solution of aldosterone (Gibco Laboratories) was prepared in ethanol diluted with culture medium and microliter quantities of the stock solution were added to the feeding medium to achieve concentrations of 10^{-7} or 10^{-4} M.

Electrical Measurements

Transepithelial DC Measurements

Methods for measuring transepithelial current and voltage were similar to those described previously (Wills & Millinoff, 1990). The transepithelial voltage (V_T) and current (I) were monitored using two pairs of Ag-AgCl wires (for chloride solutions) or 1 M NaCl agar bridges connected to Ag-AgCl wires (for nystatin experiments) leading to an automatic voltage clamp. Currents were read to within 0.01 $\mu A/cm^2$ accuracy using a digital meter and computer A/D system (Labmaster, Axon Instruments, Foster City, CA). The transepithelial conductance (G_T) was calculated from Ohm's Law using the measured deflection in V_T to an applied current pulse. The short-circuit current (I_{sc}) was either measured directly by briefly voltage clamping the epithelium to $V_T = 0$ mV, or was calculated as $V_T \cdot G_T$.

Determination of Paracellular Conductance

Paracellular conductance (G_j) or its reciprocal, paracellular resistance (R_j), was assessed using methods previously described (Wills & Millinoff, 1990). For amiloride experiments, G_j and the

cellular electromotive force (E_c) were calculated from the transepithelial resistance ($R_T = 1/G_T$) and voltage using a V_T-R_T plot method. The relationship between V_T and R_T yields a linear double intercept plot as follows (Wills, Lewis & Eaton, 1979):

$$1 = V_T/E_c + R_T/R_j. \quad (1)$$

Paracellular conductance was also estimated using nystatin. For these experiments, sodium and chloride in the mucosal solution were replaced by potassium and gluconate, respectively. Nystatin was then added to the mucosal solution at a concentration of 20–45 units/ml. V_T and R_T were analyzed in terms of Eq. (1) as above, but E_c now represents the basolateral driving force (E_{bl}) as nystatin essentially eliminated the Na^+ and Cl^- gradients across the apical membrane. The amiloride and nystatin methods have been shown to give similar estimates of G_j (Wills & Millinoff, 1990).

Transepithelial Impedance Analysis

Transepithelial impedance was measured using the methods described in Wills and Clausen (1987). A wide-band pseudo-random binary noise signal was generated digitally and converted to a constant current signal of 1.4 $\mu A/cm^2$ (peak-to-peak). Two digitization bandwidths were used to obtain good resolution at low and high frequencies. The transepithelial voltage produced in response to this signal was measured using a low noise amplifier and filtered through a 120 dB/octave low-pass anti-aliasing filter. Digitization of current and voltage signals and data acquisition were controlled by a laboratory computer with a 12 bit A-D converter (LSI 11/73 Indec Systems; Sunnyvale, CA).

Transepithelial impedance was calculated by dividing the cross-spectral density of the voltage and current, by the power spectral density of the applied current. This resulted in a set of approximately 400 linearly spaced data points for both the low and high frequency bandwidths. These 800 points were merged and reduced to 100 data points, which were logarithmically spaced in frequency from 2.2 Hz to 8.6 kHz. Each data point consisted of two numbers: a phase angle and magnitude measurement. The impedance was represented as Bode plots, which plot both phase angle and log impedance against frequency.

The data were fit by a nonlinear least squares curve fitting algorithm using morphologically-based equivalent circuit models. In these models, resistors were used to represent membrane ionic conductances and capacitors were used to represent membrane capacitances, where 1 $\mu F \simeq 1$ cm^2 membrane area (Cole, 1972). The quality of the fit to the data was evaluated by the Hamilton R-factor and the calculated standard deviations of the estimated equivalent circuit parameters. Fits yielding unusually high R-factor values or standard deviations of more than 10% of the fitted parameter value were defined as poor fits and the data excluded from further analysis. Two out of a total of 34 runs were rejected on this basis.

Statistical Analysis

All results are reported as means ± SEM. In paired experiments, each tissue served as its own control. Data were analyzed using a paired or unpaired t test or the nonparametric Mann Whitney U test for two samples where appropriate. Statistical significance was defined as $P \leq 0.05$.

Electron Microscopy

For morphologic evaluation, A6 monolayers were incubated at 28°C in sodium chloride Ringer's solution for 20 min. The A6 cultures were fixed by immersion of the filter supports in sodium chloride Ringer's solution with 0.5% glutaraldehyde for 90 min at room temperature. The filters with cells attached were then separated from the plastic insert ring and refrigerated until ready to use in a solution (450 mOsm, pH 7.4) consisting of: 1% paraformaldehyde, 5% glutaraldehyde, 0.75 mM T40 dextran, 2.5 mM calcium chloride, and 113 mM sodium cacodylate. The filters and cells were postfixed in 2% osmium tetroxide for 1 hr, stained *en block* with saturated uranyl acetate in 50% ethanol for 5 min, rapidly dehydrated in graded ethanol solutions, and embedded in Epon resin using previously described methods (Preston, Muller & Handler, 1988). Thin sections were stained with uranyl acetate and lead citrate for electron microscopy.

Results

The results are divided into three sections. First, we compare the transepithelial electrical properties of A6 epithelia and the 2F3 subclonal cell line. Next, we evaluate the effects of amiloride on these epithelia, and resolve their cellular and paracellular conductances and the net cellular driving force for Na^+ transport using equivalent circuit analysis. Lastly, we chose an appropriate equivalent circuit model for these epithelia and used impedance analysis techniques to determine the conductances and areas (measured as capacitances) of the apical and basolateral membranes.

Comparison of Transepithelial Electrical Parameters

Figure 1 compares the frequency distributions of the transepithelial potential, short-circuit current and transepithelial conductance (G_T) for A6 (filled bars) and 2F3 epithelia (open bars). V_T ranged from −11 to −93 mV for A6 epithelia with a mean of −51 ± 4 mV ($n = 38$). In contrast, V_T values for the 2F3 tissues were distributed over a higher range from −30 to −106 mV, with a significantly higher mean value of −78 ± 4 mV ($n = 34$; $P < 0.001$).

Short-circuit current values were significantly higher for the 2F3 group compared to A6. I_{sc} ranged from 5 to 45 $\mu M/cm^2$ for A6 epithelia and from 18 to 80 $\mu A/cm^2$ for 2F3 epithelia. The mean value was 27 ± 2 $\mu A/cm^2$ for A6 and was significantly higher (45 ± 3 $\mu A/cm^2$) for 2F3 ($P < 0.001$). Unlike V_T and I_{sc}, G_T values were not significantly different for the two groups. These values ranged from 0.25 to 1.17 mS/cm^2 for A6 and 0.29 to 1.27 mS/cm^2 for 2F3 (means 0.57 ± 0.04 and 0.62 ± 0.04 mS/cm^2, respectively).

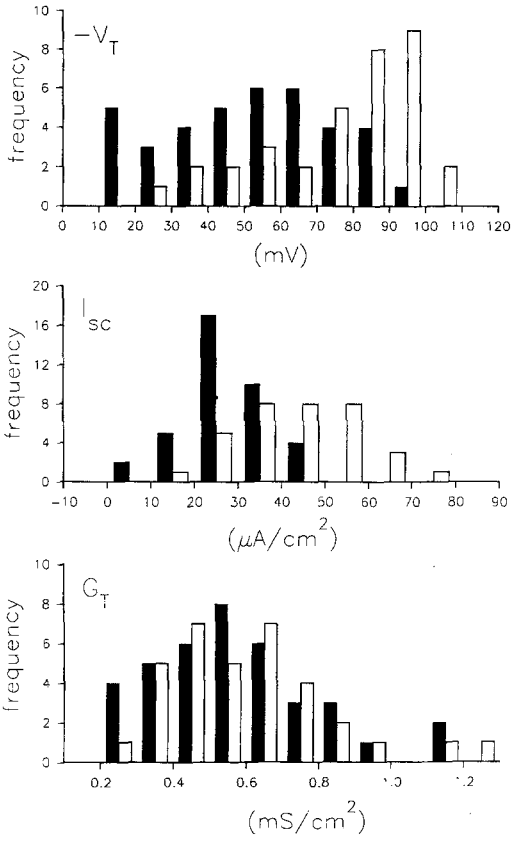

Fig. 1. Comparison of transepithelial electrical properties of A6 (filled bars, $n = 38$) and 2F3 (open bars, $n = 34$) epithelia. A6 and 2F3 monolayers had significantly different distributions for transepithelial potential (V_T) and short-circuit current (I_{sc}), but not for transepithelial conductance (G_T).

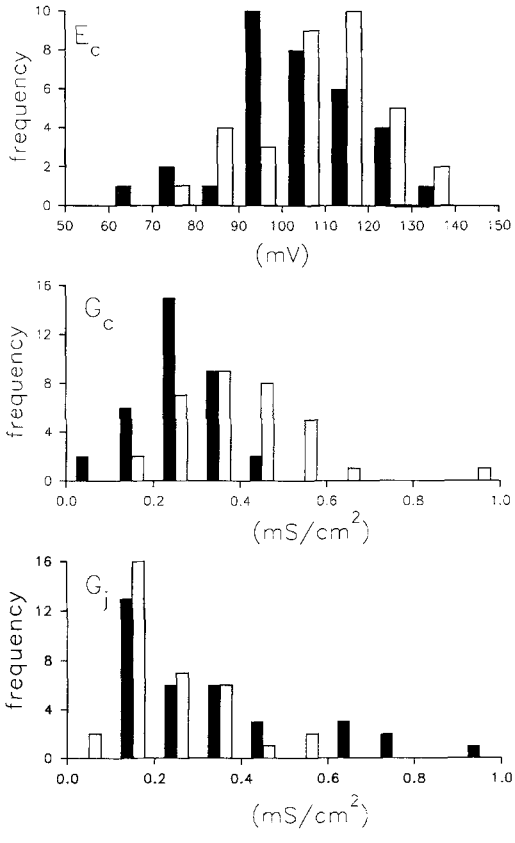

Fig. 2. Comparison of equivalent circuit parameters of A6 (filled bars) and 2F3 (open bars) epithelia. A6 and 2F3 monolayers had significantly different means for cellular conductance (G_c) and junctional conductance (G_j), but not for cellular electromotive force (E_c).

Effects of Amiloride

Table 1 summarizes the effects of amiloride (70–110 μM) added to the mucosal bathing solution. Note that for both A6 ($n = 38$) and 2F3 ($n = 34$) epithelia, amiloride resulted in a dramatic decrease in V_T and I_{sc} and a significant decrease in G_T. Although I_{sc} was less than a microampere following amiloride addition, this value was significantly different from zero for both epithelia ($P < 0.05$). Therefore, a small amount of amiloride-insensitive current was detected.

Table 1. Amiloride effects on transepithelial electrical properties

	V_T (mV)	I_{sc} ($\mu A/cm^2$)	G_T (mS/cm^2)
A6			
Control	-51 ± 4	27 ± 2	0.57 ± 0.04
Amiloride ($n = 38$)	-4 ± 1[a]	0.8 ± 0.2[a]	0.34 ± 0.04[a]
2F3			
Control	-78 ± 4[b]	45 ± 3[b]	0.62 ± 0.04
Amiloride ($n = 34$)	-4 ± 1[a]	0.8 ± 0.2[a]	0.25 ± 0.03[a]

[a] $P < 0.05$ compared to control; paired t test.
[b] $P < 0.05$ compared to A6; unpaired t test.

DC Equivalent Circuit Analysis

The paracellular (tight junctional) conductance (G_j), cellular conductance (G_c) and cellular driving force (E_c) were calculated from the response of the transepithelial potential and resistance during amiloride action (Wills et al., 1979; Wills & Millinoff, 1990; *see also* Materials and Methods). The frequency distribution of these parameters for the two types of epithelia are shown in Fig. 2, which presents a subset of the data presented in Fig. 1.

For A6 epithelia ($n = 34$), E_c ranged from 62 to

133 mV with an average value of 104 ± 3 mV (favoring net Na^+ entry). For 2F3 epithelia (n = 34), E_c ranged from 74 to 138 mV and the average value was 111 ± 2. This difference was not statistically significant. G_j values extended from 0.11 to 0.99 mS/cm^2 for A6 epithelia and between 0.07 to 0.55 mS/cm^2 for 2F3. Since these data were not normally distributed (*see* Fig. 2), a nonparametric test (the Mann-Whitney test for two samples) was used for the purposes of statistical analysis. G_j was significantly higher for A6 than 2F3 epithelia (mean values 0.33 ± 0.04 and 0.23 ± 0.02 mS/cm^2, respectively; $P < 0.05$). In contrast, G_c did appear to be normally distributed. This parameter was significantly lower for A6 compared to 2F3. These values ranged from 0.07 to 0.45 mS/cm^2 and from 0.12 to 0.94 mS/cm^2 (mean values 0.26 ± 0.10 and 0.39 ± 0.16 mS/cm^2, respectively; $P < 0.001$; unpaired t test).

Impedance Analysis

Selection of Appropriate Equivalent Circuit

As noted above, the cellular conductance were significantly different for the two groups. To further examine this difference, we used impedance analysis to resolve the apical and basolateral membrane conductances and membrane areas. As a first step in analyzing the impedance data, the distributed resistance equivalent circuit model, shown in Fig. 3*A*, was used to model the morphological features of the epithelium.

Distributed Model. The distributed circuit model was initially used by Clausen et al. (1979) to analyze the impedance properties of rabbit urinary bladder epithelium (a Na^+-transporting epithelium). The apical membrane is depicted as a parallel resistor-capacitor (RC) circuit where the resistor represents the membrane ionic conductance (G_a) and the capacitor represents the membrane capacitance (C_a), a value that is proportional to the membrane area (where 1 μF is $\simeq$ 1 cm^2 of membrane area; Cole, 1972). The basolateral membrane is represented by RC circuit elements (i.e., basolateral membrane conductance [G_{bl}] and capacitance [C_{bl}]) that are arranged in series with the apical membrane and placed along the lateral intercellular space (LIS) forming a cable-like distributed circuit. The conductance of the tight junctions (G_j) is parallel to the other membrane elements and the tight junctional area is ignored in the model since it is negligible compared to the area of the cellular pathway.

The LIS path resistance, R_p, in series with the tight junctions, is proportional to the LIS length and bathing solution resistivity and is inversely proportional to the LIS cross-sectional area. R_p is therefore a morphological indicator since changes in LIS geometry, e.g., cell swelling or shrinkage, will produce changes in R_p. Note that if the LIS is sufficiently wide, R_p will be negligible compared to the basolateral membrane impedance and the model simplifies to a lumped representation of the basolateral membrane (*cf.* Wills & Clausen, 1987).

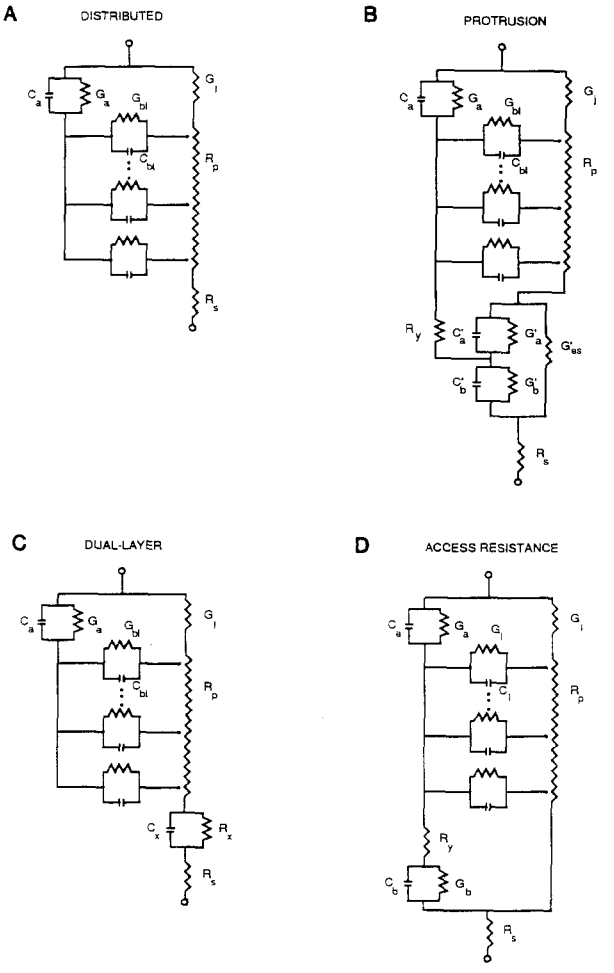

Fig. 3. Equivalent circuit models used to represent transepithelial impedance. For description, *see* text. (*A*) Distributed model. (*B*) Protrusion model. (*C*) Dual-layer model. (*D*) Access resistance model.

Figure 4 shows impedance measured in a typical epithelium bathed in NaCl Ringer's solution (circles) and after the mucosal addition of 70 μM amiloride (triangles). The smooth curves through the data show the fits by the distributed model. G_j was obtained independently using either the nystatin or amiloride method (*see* Materials and Methods). It was necessary to include an independent estimate of G_j to determine the other membrane parameters since these values cannot be calculated directly from

transepithelial impedance measurements alone (Clausen & Wills, 1981; Wills & Clausen, 1987).

The average results determined for eight A6 control tissues are summarized in Table 2. In general, the distributed model agreed with the measured data, exhibiting a mean R-factor of 0.67 ± 0.04%.

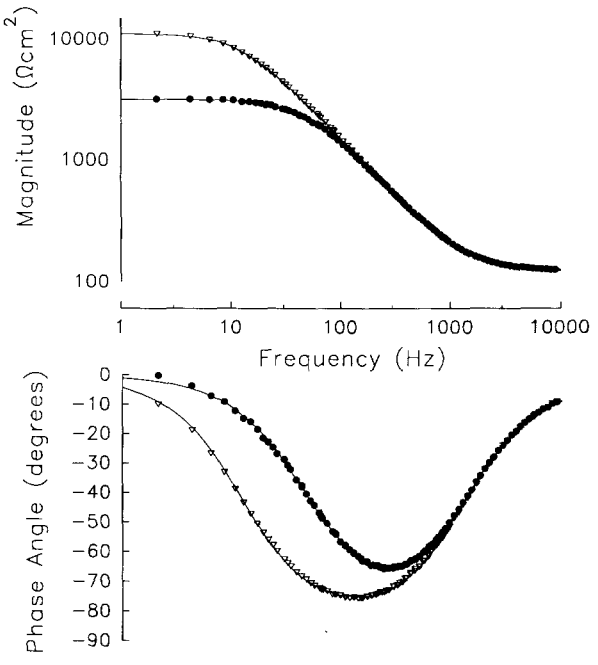

Fig. 4. Representative results from a single experiment showing Bode plots of impedance phase angle and magnitude data for control conditions (filled circles) and following mucosal application of 70 μM amiloride (inverted triangles). G_j = 0.06 mS/cm². The smooth lines are the results of fitting the data using the distributed model. The estimated membrane parameters were as follows:

	G_a mS/cm²	C_a μF/cm²	G_{bl} mS/cm²	C_{bl} μF/cm²	R_s Ωcm²	R_p Ωcm²	R-factor %
Control	0.252	1.13	8.1	7.8	120	27.4	0.59
Amiloride	0.006	1.12	6.5	11.6	118	37.8	0.51

Apical membrane capacitance values (C_a) averaged 1.05 ± 0.04 μF/cm². Since most biological membranes exhibit a specific capacitance of ~1 μF/cm² (Cole, 1972), this finding is expected for a nearly planar membrane with little infolding. In agreement with this result, little or no infolding was apparent in the apical membranes of A6 epithelia, as shown by a representative micrograph (*see* Fig. 5). The basolateral membrane capacitance measurements were also consistent with little membrane infolding and averaged 5.59 ± 0.95 μF/cm². The mean ratio of C_{bl}/C_a was 5.2 ± 0.8.

The apical membrane conductance normalized to membrane capacitance (as an index of membrane area) was 0.30 ± 0.05 mS/μF and was similar to other Na^+-transporting epithelia such as the rabbit urinary bladder (0.08 mS/μF; Clausen et al., 1979) and rabbit descending colon (0.18 mS/μF; Wills & Clausen, 1987). As indicated in Fig. 4, addition of amiloride reduced G_a. The normalized apical membrane conductance G_{a-n} significantly decreased to 0.12 ± 0.04 mS/μF (n = 8; $P < 0.003$). This finding is expected for a Na^+-transporting epithelium.

Despite the above reasonable estimates of the distributed model for the apical and basolateral capacitance and the apical membrane conductance, estimates of basolateral membrane conductances were considerably larger than previous studies and averaged 10.0 ± 1.4 mS/cm². In terms of this model, the membrane resistance ratio (α) measured using microelectrodes is a function of R_p and R_s as well as the apical and basolateral membrane conductances. Using the following equation which assumes that R_s is equally distributed on both sides of the epithelium, α can be calculated as (Clausen et al., 1979)

$$\alpha = (R_a + R_s/2)/(\sqrt{R_{bl}R_p}\coth\sqrt{R_p/R_{bl}} + R_s/2). \quad (2)$$

For A6 epithelia under control conditions, α averaged 20 ± 3 (n = 8). This value is much higher than previous microelectrode measurements by

Table 2. Comparison of impedance circuit models for A6 and 2F3 epithelia

	G_a (mS/cm²)	C_a (μF/cm²)	G_{bl} (mS/cm²)	C_{bl} (μF/cm²)	R_p (Ωcm²)	R_s (Ωcm²)	C_s (μF/cm²)	R_s (Ωcm²)	R-factor (%)
A6 (n = 8)									
Distributed	0.31 ± 0.04	1.05 ± 0.04	10.0 ± 1.4	5.59 ± 0.95	53.6 ± 6.4	—	—	—	0.67 ± 0.04
Dual-layer	0.37 ± 0.07	1.27 ± 0.07	3.0 ± 0.4	4.67 ± 0.58	30.9 ± 4.0	42.4 ± 12.8	6.90 ± 1.86	—	0.41 ± 0.04
Access resistance	0.37 ± 0.08	1.24 ± 0.08	3.0 ± 0.4	4.52 ± 0.66	43.2 ± 6.5	—	—	196 ± 330	0.41 ± 0.04
2F3 (n = 4)									
Distributed	0.55 ± 0.12	1.07 ± 0.06	12.2 ± 3.1	4.89 ± 1.75	53.2 ± 16.8	—	—	—	0.70 ± 0.06
Dual-layer	0.79 ± 0.23	1.43 ± 0.04	3.5 ± 1.7	4.23 ± 1.98	30.8 ± 8.0	35.3 ± 8.2	4.50 ± 1.08	—	0.40 ± 0.04
Access resistance	0.79 ± 0.23	1.42 ± 0.03	3.5 ± 1.7	4.16 ± 1.98	68.8 ± 24.4	—	—	237 ± 75	0.40 ± 0.04

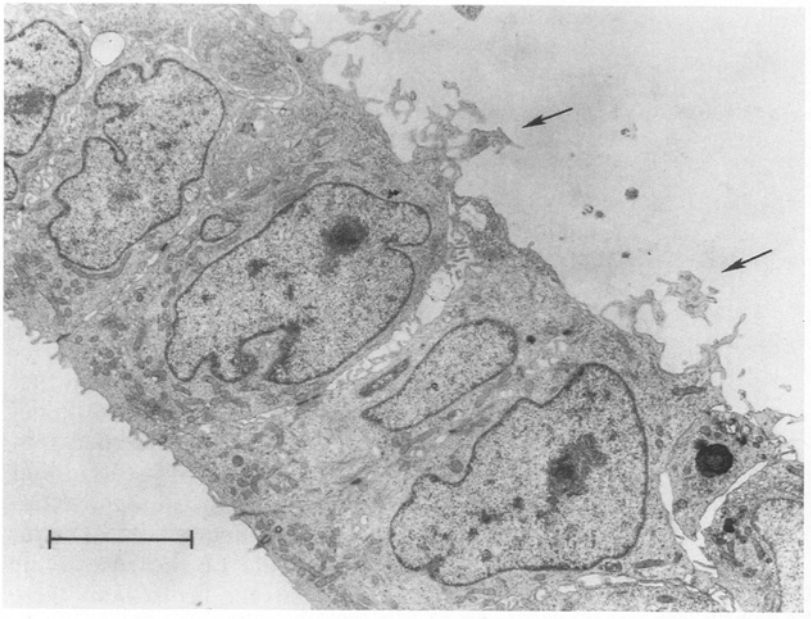

Fig. 5. Electron micrograph of A6 monolayer (passage 79; day 14) grown on a permeable filter support (Millicell-HA). Arrows denote the cytoplasm-filled protrusions of the basolateral membrane into the support. Calibration bar = 5 μm. (Electron microscopy is by courtesy of M.D. Christensen.)

Granitzer et al. (1991; α = 4) and Thomas and Mintz (1987; α = 5-7). Two possible explanations for this discrepancy are: (i) possible damage to the apical membrane by the microelectrode impalements, i.e., a microelectrode-induced apical membrane shunt conductance or (ii) possible inaccuracy in the analysis of the basolateral membrane impedance by the distributed model due to the electrical properties of some unaccounted for morphological feature of the epithelium. Since the careful studies of Granitzer et al. (1991) made the first explanation unlikely, we assessed the second possibility.

Basolateral Membrane Protrusions Model. Examination of micrographs of A6 epithelium (*see* Fig. 5) revealed a morphological feature that was previously reported by Cereijido et al. (1978) and Cook et al. (1989) for MDCK monolayers grown on permeable supports. Both A6 and MDCK epithelia extend narrow cytoplasm-filled projections of the basal membrane into the microporous support.

Figure 3*B* is an equivalent-circuit model that explicitly considers the impedance of the basal protrusions. In essence, the protrusions are treated like a second independent cell layer. G'_a and G'_b represent its apical and basolateral membrane conductances, respectively, and C'_a and C'_b represent the respective membrane capacitances. A high-conductance extracellular space pathway around the protrusions is represented by G'_{es}. Finally, intracellular current from the epithelium can gain access to the serosal layer via R_y, the resistance of the intracellular solution penetrating the pores. Considering the good agreement already observed between the distributed model (Fig. 3*A*) and the experimental data (*see* Fig. 4), this circuit is certainly far too complex to be useful in analyzing transepithelial impedance. However, two limiting cases can be considered, which dramatically simplify the analysis.

Case I: Dual-layer model. We first consider the case when R_y is large (compared to the epithelial basolateral impedance) such that no significant intracellular current flows from the epithelium into the protrusions. This is a reasonable possibility for two reasons. First, the diameter of the basolateral membrane protrusions is small (~0.5 μm) compared to the cell diameter (~7.5 μm). Second, the impedance of the epithelial basolateral membrane dramatically decreases with increasing frequency (due to the membrane capacitance), hence at all but the lowest frequencies, one could expect that the impedance of the protrusions would be significantly less than R_y. In this case, the protrusions would impede mainly the extracellular current, and they can be considered as an electrically isolated serosal cell layer possessing a high paracellular conductance. The equivalent-circuit model for this situation is identical to that used by Clausen, Reinach and Marcus (1986) in impedance studies of the cornea, a tight epithelium in series with an underlying leaky epithelium (the corneal endothelium). Lim and Fishbarg (1981) showed that the transepithelial electrical properties of a leaky epithelium can be represented by a single parallel RC circuit. Hence the circuit shown in Fig. 3*B* simplifies to that shown in Fig. 3*C*. We refer to this as the "dual-layer" model.

To assess this model, we first determined whether the quality and accuracy of the data justified

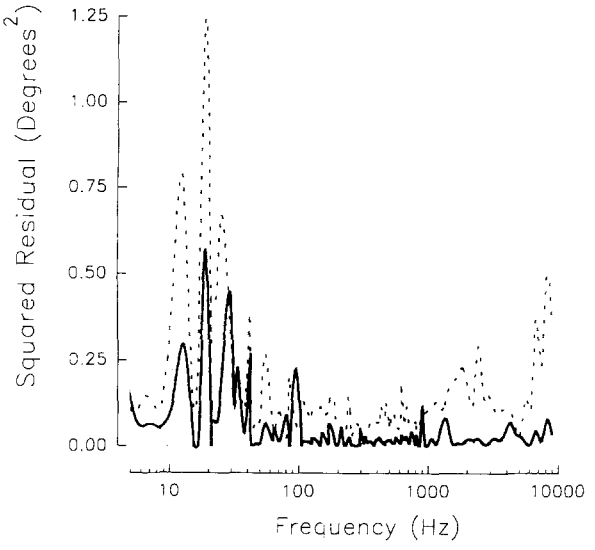

Fig. 6. Mean squared phase angle residual errors *versus* frequency for eight control A6 epithelia. The upper (dotted) line shows the residual error for the distributed model and the lower (solid) line shows the error for the dual-layer model. On average over the entire frequency range, the dual-layer model reduced the sum of the squared residual errors by a factor of 7.4 ± 0.7 (n = 95 frequencies).

the inclusion of the additional circuit parameters, namely R_x and C_x, the effective resistance and capacitance of the basolateral membrane protrusions. Three independent methods were used to evaluate this issue. First, we compared the best-fit residual errors (i.e., the difference between the measured impedance and the impedance predicted by the best-fit results from the models) for the dual-layer and the distributed models. Second, an F test (variance ratio) analysis was performed to determine whether the reduction in the variance achieved by the dual-layer model was statistically significant. Lastly, we examined the asymptotic estimates of the standard deviations of R_x and C_x to ensure that these two parameters were well determined by the data.

Figure 6 shows the mean squared phase angle residual errors for eight (A6) epithelia. The upper (dotted) line shows the residual error for the distributed model and the lower (solid) line shows the error for the dual-layer model. On average over the entire frequency range, the dual-layer model reduced the sum of the squared residual errors by a factor of 7.4 ± 0.7 (n = 95 frequencies). The average R-factor for the dual-layer model was 0.41 ± 0.03% (n = 8), lower than that for the distributed model (0.67 ± 0.04%, *see above*). The reduction in the residual error by the dual-layer model was highly significant as indicated by variance ratio analysis (F = 89.0; df = 92; $P < 10^{-7}$). Parameter standard deviations for R_x and C_x averaged 2.2 ± 0.7% and 1.3 ± 0.3% of the parameter values, respectively, indicating that these parameters are well determined from the available data.

As indicated in Table 2, apical membrane parameters and the basolateral membrane capacitance estimated by the dual-layer model did not significantly differ from those calculated using the distributed model. In contrast, G_{bl} was significantly lower by ~70%. When the resistance R_x on the serosal side of the epithelium is taken into account, the calculated membrane resistance ratio α averaged 8 ± 2 [*cf.* Clausen et al. (1986) for equations describing α]. This value was significantly lower than that calculated for the distributed model and was comparable to previous microelectrode measurements.

Case II: Access resistance. In the second limiting case, we consider the possibility that the extracellular conductance (G'_{es}) around the cell protrusions is negligible. This would be the case if the extracellular spaces between the protrusions were large and highly conductive. Under these conditions, Fig. 3*B* simplifies to the equivalent circuit seen in Fig. 3*D*. We refer to this as the "access resistance" model.

In this model, the basolateral membrane lining the lateral spaces, as well as that which rests flat on the filter support, has conductance and capacitance described by G_l and C_l, respectively; the basal membrane protrusions have conductance and capacitance described by G_b and C_b, respectively. The total basolateral membrane electrical properties are defined as the sum of the respective conductances and capacitances (i.e., $G_{bl} = G_l + G_b$ and $C_{bl} = C_l + C_b$). Although the access resistance model has three more circuit elements than the distributed model, we effectively reduce the number of circuit parameters by assuming that the specific conductance of the basal protrusions is the same as the other regions of basolateral membrane. Thus, C_b can be calculated as $C_b = C_l G_b / G_l$.

The transepithelial impedance of the access-resistance model is described by

$$Z_t = \frac{Y_a + Y_b + Y'_l + G_l[R_p(Y_a + Y_b)Y'_l/Y_l + 2(1\text{-sech}\sqrt{Y_l R_p})] + R_s}{Y_a(Y_b + Y'_l) + G_l[Y_a + Y_b + Y'_l + R_p Y_a Y_b Y'_l/Y_l]} \tag{3}$$

where $Y'_l = \sqrt{Y_l/R_p}\ \tanh\sqrt{Y_l R_p}$. The admittances of the apical membrane (Y_a), basolateral membrane (Y_l), and basal protrusions (Y_b) are given by

$$Y_a = G_a + j\omega C_a,\ Y_l = G_l + j\omega C_l,\ Y_b = G_b + j\omega C_b/[1 + R_x(G_b + j\omega C_b)] \tag{4}$$

where ω is the angular frequency ($2\pi f$), and $j = \sqrt{-1}$.

Table 3. Amiloride effects on impedance properties

	G_a (mS/cm²)	C_a (μF/cm²)	G_{bl} (mS/cm²)	C_{bl} (μF/cm²)	α	I_{sc} (μA/cm²)
A6 (n = 8)						
Control	0.37 ± 0.08	1.27 ± 0.07	2.95 ± 0.40	4.67 ± 0.58	8 ± 2	27 ± 2
Amiloride	0.11 ± 0.04	1.13 ± 0.05	4.00 ± 0.63	8.79 ± 1.01	84 ± 56	0.4 ± 0.3
Difference	−0.26 ± 0.06[a]	−0.14 ± 0.06	1.06 ± 0.74	4.13 ± 0.82[a]	67 ± 54	27 ± 2[a]
2F3 (n = 4)						
Control	0.79 ± 0.23	1.43 ± 0.04	3.48 ± 1.67	4.23 ± 1.98	6 ± 4	51 ± 3
Amiloride	0.13 ± 0.04	1.24 ± 0.09	2.85 ± 1.24	6.30 ± 2.08	46 ± 32	2 ± 0.5
Difference	−0.66 ± 0.19[a]	−0.19 ± 0.12	−0.63 ± 1.60	2.07 ± 0.78	41 ± 29	46 ± 4[a]

[a] $p < 0.05$; paired t test.

Like the dual-layer model, the access-resistance model has two more circuit parameters (R_y and G_b) than the distributed model, which must be determined by the available impedance data. Table 2 shows results obtained from fitting the model to the data. In all cases, the model produced a significant reduction ($P < 0.05$) in the residual error, compared to the distributed model, as determined by an F test; the mean R-factor was 0.4 ± 0.04%. Also similar to the dual-layer model, membrane resistance ratios predicted by the access resistance model were significantly lower than those predicted by the distributed model. For the access resistance model, the resistance ratio is defined by

$$\alpha = (1/G_a + R_s/2)/(1/G_{bl} + R_s/2) \quad (5)$$

where

$$G_{bl} = G_b/(1 + R_y G_b) + \sqrt{G_l/R_p}\tanh\sqrt{G_l R_p}. \quad (6)$$

This ratio averaged 8 ± 2, a value comparable to measurements obtained from microelectrode studies. Finally, for control conditions in both A6 and 2F3 epithelia, the access resistance model produced estimates of G_a, C_a, G_{bl}, and C_{bl} (*see* Table 2) that were not statistically different from those determined by the dual-layer model, although R_p values were slightly, but significantly, larger ($P < 0.03$; paired t test). The basolateral protrusions had a similar conductance (G_b) and capacitance (C_b) to the basolateral membrane (G_l). The mean G_b was 1.54 ± 0.30 mS/cm² compared to 1.43 ± 0.21 mS/cm² for G_l. Both C_b and C_l were equal to 2.2 ± 0.4 μF/cm². Therefore, similar specific conductances were observed for the protrusions and basolateral membrane.

In some cases (i.e., under other experimental conditions such as amiloride), we were unable to obtain reasonable parameter estimates when fitting data by the access resistance model (results not shown). The reasons for this are unclear, but this problem was not observed when using the dual-layer model.

Summary of models. The dual-layer and access resistance models are limiting simplifications of Fig. 3*B*, a morphologically-based equivalent-circuit model that explicitly considers the effects of observed basal protrusions into the support membrane. In the dual-layer model, the protrusions are assumed to impede only extracellular current exiting the lateral spaces; in the access resistance model, the protrusions are assumed to impede only the small amount of intracellular current gaining access to the protrusions via the intracellular pore access resistance. Both models produced significant reductions in the residual error, compared with fits by the distributed model, indicating that the quality and amount of data are sufficient to determine values for the additional circuit elements. Both models also produced similar estimates for apical and basolateral membrane parameters (*see* Table 2). Finally, both models yielded resistance-ratio estimates (α) that were comparable to values measured using microelectrode techniques. In the results that follow, results will be reported based on fits by the dual-layer model.

Comparison of the Impedance Properties of A6 and 2F3 Epithelia

As summarized in Table 2, 2F3 cells had a higher apical membrane conductance compared to A6 cells (mean G_a = 0.79 ± 0.23 mS/cm² and 0.37 ± 0.08 mS/cm², respectively). Despite a significantly larger variability in G_a for the 2F3 epithelium, this difference reached statistical significance (P = 0.05). In contrast, G_{bl}, C_a, and C_{bl} did not significantly differ between the two groups. G_{bl} averaged approximately 3 mS/cm², or approximately 0.7 mS/μF. This value is similar to previous estimates for other tight epithelia (*cf.* Wills & Clausen, 1987). As discussed above for the distributed model, C_a and C_{bl} averaged approximately 1 and 4–5 μF/cm².

Effects of Amiloride on Membrane Impedance

As previously discussed (for the distributed model) and now shown for the dual-layer model in Table 3, G_a was significantly decreased by mucosal amiloride addition. In some cases, G_a approached zero following drug addition. Unlike the control condition, in the presence of amiloride, G_a was not significantly different for the two epithelia. The membrane resistance ratio was increased in all experiments consistent with a reduction in the apical membrane conductance. G_{bl} and C_a were not significantly altered by amiloride. C_{bl}, was variable and tended to increase following amiloride, but this effect reached statistical significance only for A6 epithelia. The reason for the increase in C_{bl} was unclear.

Discussion

The results extend our previous findings of a large amiloride-sensitive Na^+ current across A6 epithelium (Wills & Millinoff, 1990) and confirm increased Na^+ transport rates across the cloned A6 cell line, 2F3 (Verrey et al., 1987; Wills & Millinoff, 1990). More importantly, new information has been obtained concerning the membrane properties of these two epithelia. In the following sections, we will first compare the transepithelial electrical properties of these two epithelia and identify differences with respect to cellular driving forces, and cellular and paracellular resistances. Next, we will discuss and verify the use of an appropriate morphologically based equivalent circuit model for analysis of transepithelial impedance results. Lastly, we will compare impedance estimates of apical and basolateral membrane properties for the two epithelia.

Comparison of Transepithelial Electrical Properties

In agreement with Verrey et al. (1987), we observed that V_T and I_{sc} were significantly different for 2F3 than A6 epithelia. However, G_T values were similar for the two epithelia. The latter result would not be expected if the apical membrane Na^+ conductance was the only difference between the two tissues. To further compare these epithelia, DC equivalent circuit analysis techniques were used to analyze the response of V_T and G_T to mucosal amiloride application. As described above (*see* Materials and Methods), this analysis yields estimates of the cellular driving force (E_c), cellular conductance (G_c) and paracellular (tight junctional) conductance (G_j). As indicated in Fig. 2, the average cellular driving force E_c was not significantly different for the two epithelia.

An unexpected finding was that the paracellular conductance was lower for 2F3 epithelia compared to A6 epithelia. This may partly account for the relatively higher transepithelial potential for 2F3 epithelia. Interestingly, the differences in V_T and G_j for the two epithelia resulted in similar amounts of current transversing the paracellular and cellular pathways under open-circuit conditions. This paracellular current, calculated as $I_j = V_T \cdot G_j$, equaled 11.6 $\mu A/cm^2$ for A6 and 13.2 $\mu A/cm^2$ for 2F3 epithelia. Under open-circuit conditions, the paracellular current is equivalent to the cellular current (i.e., $I_j = I_c$). Therefore, the two epithelia had similar transcellular Na^+ transport rates under these conditions. It is tempting to speculate that the comparable rates of transport result in similar amounts of Na^+ delivery to the basolateral membrane Na-K ATPase. Therefore, little difference in basolateral membrane properties would be expected for the two epithelia.

Membrane Impedance Properties: Verification of Morphologically-Based Equivalent Circuit Model

The present study is the first impedance study of a cultured epithelial monolayer. A potential advantage of such a cell culture model system is its inherent morphological simplicity since no additional cell layers such as smooth muscle or connective tissue are present to complicate the analysis. For this reason, we initially fitted the data using a simple distributed model. As mentioned above (*see* Results), when the LIS is sufficiently wide, this model becomes equivalent to a simple lumped representation. Although this model provided fits to the data that had the lowest residual error values of any epithelia yet studied, the resulting estimates of membrane resistance parameters grossly disagreed with available microelectrode estimates (Thomas & Mintz, 1987; Granitzer et al., 1991).

Inspection of electron micrographs of A6 and 2F3 epithelia revealed a relatively smooth apical membrane. We note that this finding is in contrast to the recent reports of Tousson et al. (1989) who found "tufts" of microvilli in this membrane for A6 cells. The reason for this difference is unknown, and it is unclear whether the tissues in the two studies were similar with respect to age or passage number.

A striking feature of A6 cells were small cytoplasm-filled basal membrane intrusions into the underlying filter. Since these small fluid-filled spaces would be expected to have resistive and capacitive properties, the impedance data was analyzed using two models that incorporated this feature. Both of these models provided similar estimates of apical

membrane properties, membrane resistance ratios that agree with available microelectrode estimates and produced significantly better fits to the data.

Predictions of R_p

As a first step in evaluating the validity of the above models, we assessed whether the dual-layer model provided physiologically reasonable values for the LIS resistance (R_p). By treating the apical surface of the cell as a simple square, we calculated the width of the LIS from the paracellular resistance using the following equations (Clausen et al., 1979):

$$R_p = R_p^{cell}/N^{cell} \quad (7)$$

$$R_p^{cell} = (H_c/A_{LIS}^{cell})R \quad (8)$$

$$A_{LIS}^{cell} = 4(W_L/2)W_c = 2W_L W_c \quad (9)$$

where R_p^{cell} is the LIS resistance for a single cell, N^{cell} is the total number of cells/cm^2, H_c is cell height, R is solution resistivity, A_{LIS}^{cell} is the area of the LIS for each cell, W_L is the width of the LIS, and W_c is the width of the cell. (Note that the above equations assume that the LIS has a simple geometry. If the LIS has significant tortuosity, its width will be underestimated.)

We have previously measured the number of cells in a typical tissue culture insert as 1.8×10^6 cell/cm^2 (B. Jovov, N.K. Wills & S.A. Lewis, *submitted*). R was approximately 150 Ωcm for the amphibian NaCl Ringer's solution. W_c (7.5 μm) and H_c (15 μm) were measured in vitro with the same solution using optical methods (W.E. Crowe and N.K. Wills, *submitted*). Cells heights of 15–20 μm have been previously reported for MDCK epithelia from confocal microscopy experiments by Ballacao and Stelzer (1989). [*Note:* The fixative solution used for the electron micrographs shown in Fig. 5 was hypertonic and may have possibly caused some decrease in cell height.]

To estimate LIS width, we used the combined mean R_p value for A6 and 2F3 epithelia (31 Ωcm^2). W_L or width of the lateral intercellular space was then calculated as 27 nm. This value is nearly four times wider than that calculated for the rabbit urinary bladder (7 nm) and suggests a relatively wide LIS for A6 or 2F3 epithelium.

Membrane Conductances and I_{sc}

Although the membrane resistance ratios for the dual-layer model agree well with previous microelectrode measurements, there is an apparent discrepancy concerning estimates of individual membrane resistances. For example, Granitzer et al. (1991) estimated the mean apical and basolateral membrane conductances as 80 and 292 μS/cm^2, respectively, whereas the present study estimated the same parameters as 370 and 2950 μS/cm^2 for A6 epithelia and 790 and 3480 μS/cm^2 for 2F3 epithelia. In part, these differences can be accounted for by differences in Na^+ transport rates in the two studies. Granitzer et al. (1991) reported a mean amiloride-sensitive I_{sc} of ~4 μA/cm^2, whereas the mean amiloride-sensitive I_{sc} for A6 epithelia in the present study was 27 μA/cm^2 and 44 μA/cm^2 for 2F3 epithelia. Therefore, larger apical membrane conductances would be expected for the present study. In this regard, it is also noteworthy that G_a decreased following amiloride addition, consistent with the notion that G_a is decreased when I_{sc} is low. Impedance analysis estimates of basolateral membrane conductance were also higher than those reported by Granitzer et al. (1991). In this regard it is important to note that Granitzer et al. experiments were performed under short-circuit conditions whereas the present study used open-circuit conditions. Therefore, the distribution of intracellular ions and other factors may also differ between the two studies.

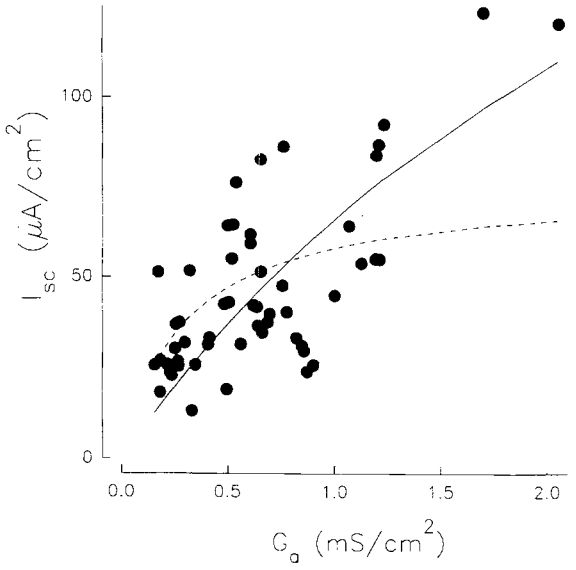

Fig. 7. Short-circuit current (I_{sc}) as a function of apical conductance (G_a). The smooth curves are the results of fits of the data by Eq. (13) using two different values for G_{bl} (dashed line: G_{bl} = 0.3 mS/cm^2; solid line: G_{bl} = 3.3 mS/cm^2).

To further evaluate the relationship between membrane conductances and the short-circuit current, we next pooled apical membrane conductance data for A6 and 2F3 epithelia (*see* Fig. 7). For reasons that will become clear below, we also included additional data obtained from epithelia grown in the presence of aldosterone (R.K. Purcell, C. Clausen and N.K. Wills, *in preparation*).

As in previous studies of conductive Na^+ transport in tight epithelia (e.g., Clausen et al. 1979), I_{sc} increased with G_a. In contrast, I_{sc} was uncorrelated with G_{bl} (*data not shown*) and G_{bl} showed considerable scatter. Previous authors (Kottra & Fromter, 1984) have noted similar difficulties in determining individual membrane conductances. For this reason, we independently evaluated G_{bl} from the relationship between G_a and I_{sc}.

Verification of G_{bl}

Under short-circuit conditions, V_{bl} is equal to $-V_a$ and the short-circuit current is defined as follows:

$$I_{sc} = (E_a - V_a)/R_a = (E_{bl} + V_a)/R_{bl} \quad (10)$$

and

$$V_a = E_a R_{bl}/(R_a + R_{bl}) - E_b R_a/(R_a + R_{bl}). \quad (11)$$

Substituting Eq. (10) into Eq. (1) and converting the resistances to conductances

$$I_{sc} = (E_a + E_{bl}) G_a G_{bl}/(G_a + G_{bl}). \quad (12)$$

If we define $E_c = E_a + E_{bl}$ and define the maximum short-circuit current as $i_{max} = G_{bl}(E_c)$, then this relationship can be treated as a Michaelis-Menten equation

$$I_{sc} = (G_a i_{max})/(G_a + G_{bl}) = G_a(G_{bl}E_c)/(G_a + G_{bl}) \quad (13)$$

and G_{bl} can be computed as the point at which I_{sc} is half-maximal.

Because of the inherent scatter in the G_a data, it was useful to include tissues with higher I_{sc} values before evaluating the predictions of the above equation. For this reason, results from aldosterone-treated tissues were also used (*see above*). The smooth curves shown in Fig. 7 are the results of fitting of the data using Eq. (13) and the G_{bl} value of Granitzer et al. (1991; dotted line: G_{bl} = 0.3 mS/cm^2) and the combined mean value from the present impedance data (solid line: $G_{bl} = 3.3 \pm 0.3$ mS/cm^2; $n = 54$). Note that the relationship predicted from the lower estimate of G_{bl} misfits the data at high I_{sc} values. In contrast, the higher G_{bl} value was able to fit the data over the entire I_{sc} range. Therefore, our G_a and I_{sc} data are internally consistent with a relatively high G_{bl}.

The mean cellular driving force (E_c) determined by the latter fit was 86 ± 4 mV. Given the scatter in the data, this value is in good agreement with the combined mean E_c value of 110 mV for A6 and 2F3 experiments. The results of the fit using the lower value for G_{bl} (0.3 mS/cm^2), however, estimated E_c as 251 mV. This value is more than twice that of previous estimates (Wills & Millinoff, 1990).

Conclusions

In summary, impedance analysis of Na^+ transporting cultured renal epithelia has confirmed the presence of an amiloride-sensitive conductance in the apical membrane and provided new information concerning membrane areas and basolateral membrane properties. In epithelia grown from the A6 cell line and the subclonal A6 cell line, 2F3, the apical membrane conductance was correlated with the transepithelial short-circuit current. In contrast, the basolateral membrane conductance showed little relationship to the transepithelial Na^+ transport rate and was more variable. The ratio of apical to basolateral membrane areas (measured as capacitances) and the predicted LIS width were physiologically reasonable and consistent with the morphology of the epithelium. An unexpected finding was a significant RC component in series with the apical and basal membrane impedance. This additional barrier could affect DC measurements of basolateral membrane properties and may reflect basal membrane protrusions into the underlying filter paper support. In addition, higher Na^+ transport rates were observed in 2F3 epithelia than in A6 epithelia. The 2F3 epithelia had a significantly higher apical membrane conductance and lower paracellular conductance than A6 epithelia. Consequently, the higher Na^+ transport across 2F3 epithelia is likely to reflect a difference in Na^+ channel turnover, expression, or activity. Tight junctions may also be established or regulated in a different manner for the two epithelia. Therefore, by comparing the 2F3 and A6 cell lines, important insights might be gained concerning the interrelationship between tight junctions and transport proteins in epithelial organization and function.

We wish to thank Dr. B. Rossier for his help and generous donation of 2F3 cell line. Thanks are also due to Drs. W. Crowe and S. Lewis for their comments on this manuscript, to M.D. Christensen who kindly provided the micrograph of A6 epithelium, and to Drs. B. Jovov, S. Lewis and P. Donaldson for their contributions to the data. We are also grateful to L. Millinoff and D. Eldridge for technical assistance. This work was supported by N.I.H. grant #DK 29962 to N.K. Wills.

References

Bacallao, R., Stelzer, E.K. 1989. Preservation of biological specimens for observation in a confocal fluorescence microscope and operational principles of confocal fluorescence microscopy. *Methods Cell Biol.* **31**:437–452

Cereijido, M., Robbins, E.S., Dolan, W.J., Rotunno, C.A.,

Sabatini, D.D. 1978. Polarized monolayers formed by epithelial cells on a permeable and translucent support. *J. Cell Biol.* **77**:853–880

Clausen, C., Lewis, S.A., Diamond, J.M. 1979. Impedance analysis of a tight epithelium using a distributed resistance model. *Biophys. J.* **26**:291–318

Clausen, C., Machen, T.E., Diamond, J.M. 1983. Use of AC impedance analysis to study membrane changes related to acid secretion in amphibian gastric mucosa. *Biophys. J.* **41**:167–178

Clausen, C., Reinach, P.S., Marcus, D.C. 1986. Membrane transport parameters in frog corneal epithelium measured using impedance analysis techniques. *J. Membrane Biol.* **91**:213–225

Clausen, C., Wills, N.K. 1981. Impedance analysis in epithelia. *In:* Ion Transport by Epithelia. S.G. Schultz, editor. Raven, New York

Cole, K.S. 1972. Membranes, Ions, and Impulses. University of California Press, Berkeley

Cook, J.R., Crute, B.E., Patrone, L.M., Gabriels, J., Lane, M.E., Van Buskirk, R.G. 1989. Microporosity of the substratum regulates differentiation of MDCK cells in vitro. *In Vitro Cell Dev. Biol.* **25**:914–922

Fidelman, M.L., Watlington, C.O. 1987. Effect of aldosterone and insulin on mannitol, Na^+ and Cl^- fluxes in cultured epithelia of renal origin (A6): Evidence for increased permeability in the paracellular pathway. *Biochim. Biophys. Acta* **931**:205–214

Granitzer, M., Leal, T., Nagel, W., Crabbe, J. 1991. Apical and basolateral conductance in cultured A6 cells. *Pfluegers Arch.* **417**:463–468

Hamilton, K.L., Eaton, D.C. 1985. Single-channel recordings from amiloride-sensitive epithelial sodium channel. *Am. J. Physiol.* **249**:C200–C207

Handler, J.S., Preston, A.S., Perkins, F.M., Matsumura, M., Johnson, J.P., Watlington, C.O. 1981. The effect of adrenal steroid hormones on epithelia formed in culture by A6 cells. *Ann. N.Y. Acad. Sci.* **372**:442–454

Kottra, G., Fromter, E. 1984. Rapid determination of intraepithelial resistance barriers by alternating current spectroscopy. II. Test of model circuits and quantification of results. *Pfluegers Arch.* **402**:421–432

Lang, M.A., Muller, J., Preston, A.S., Handler, J.S. 1986. Complete response to vasopressin requires epithelial organization in A6 cells in culture. *Am. J. Physiol.* **250**:C138–C145

Lim, J.J., Fischbarg, J. 1981. Electrical properties of rabbit corneal endothelium as determined from impedance measurements. *Biophys. J.* **36**:677–695

Olans, L., Sariban-Sohraby, S., Benos, D.J. 1984. Saturation behavior of single amiloride-sensitive Na^+ channels in planar lipid bilayers. *Biophys. J.* **46**:831–835

Perkins, F.M., Handler, J.S. 1981. Transport properties of toad kidney epithelia in culture. *Am. J. Physiol.* **241**:C154–C159

Preston, A.S., Muller, J., Handler, J.S. 1988. Dexamethasone accelerates differentiation of A6 epithelia and increases response to vasopressin. *Am. J. Physiol.* **255**:C661–C666

Thomas, S.R., Mintz, E. 1987. Time-dependent apical membrane K^+ and Na^+ selectivity in cultured kidney cells. *Am. J. Physiol.* **253**:C1–C6

Tousson, A., Alley, C.D., Sorscher, E.J., Brinkley, B.R., Benos, D.J. 1989. Immunochemical localization of amiloride-sensitive sodium channels in sodium-transporting epithelia. *J. Cell Sci.* **93**:349–362

Verrey, F., Schaerer, E., Zoerkler, P., Paccolat, M.P., Geering, K., Kraehenbuhl, J.P., Rossier, B.C. 1987. Regulation by aldosterone of Na^+, K^+-ATPase mRNAs, protein synthesis, and sodium transport in cultured kidney cells. *J. Cell Biol.* **104**:1231–1237

Wills, N.K., Clausen, C. 1987. Transport-dependent alterations of membrane properties of mammalian colon measured using impedance analysis. *J. Membrane Biol.* **95**:21–35

Wills, N.K., Lewis, S.A., Eaton, D.C. 1979. Active and passive properties of rabbit descending colon: A microelectrode and nystatin study. *J. Membrane Biol.* **45**:81–108

Wills, N.K., Millinoff, L.P. 1990. Amiloride-sensitive Na^+ transport across cultured renal (A6) epithelium: Evidence for large currents and high Na:K selectivity. *Pfluegers Arch.* **416**:481–492

Wills, N.K., Millinoff, L.P., Crowe, W.E. 1991. Na^+ channel activity in cultured renal (A6) epithelium: Regulation by solution osmolarity. *J. Membrane Biol.* **121**:79–90

Received 13 June 1991; revised 6 September 1991